Powder Technology 286 (2015) 654–667

Contents lists available at ScienceDirect

Powder Technology

journal homepage: www.elsevier.com/locate/powtec

Fluidized-bed melt granulation: The effect of operating variables on process performance and granule properties

Sussy Veliz Moraga [a], Marta P. Villa [b], Diego E. Bertín [b], Ivana M. Cotabarren [b], Juliana Piña [b], Marisa Pedernera [b], Verónica Bucalá [b,*]

[a] Centro de Investigación Tecnológica del Agua y en el Desierto, Ceitsaza, Universidad Católica del Norte, Avenida Angamos 0610, Antofagasta, Chile
[b] Departamento de Ingeniería Química (Universidad Nacional del Sur) and Planta Piloto de Ingeniería Química (UNS-CONICET), Camino La Carrindanga Km. 7, 8000, Bahía Blanca, Argentina

ARTICLE INFO

Article history:
Received 10 January 2015
Received in revised form 13 August 2015
Accepted 2 September 2015
Available online 8 September 2015

Keywords:
Melt granulation
Fluidized bed
Urea
Growth mechanisms
Coating
Agglomeration

ABSTRACT

This paper addresses fluid-bed melt granulation (FBMG) for seeds and a binder of the same chemical nature, i.e. with an identical melting point. The purpose of this work is to study the impact of seed size, bed temperature, binder flowrate, and fluidization and atomization air flowrates on process parameters, such as mass balance closure, fines deposited on granulator walls and granulation efficiency, and on product properties, such as particle size distribution, percentages of particles effectively coated or agglomerated and granule crushing strength, among others. This is done to find the operating regions capable of avoiding lump formation or out-of-specification granule production. This work is focused on operating conditions and seed diameter ranges not addressed before. In particular, relatively large seed particles compared to the size of the droplets, high binder/seed mass ratios, and bottom spray are used. The specific method proposed to characterize the granular product into three categories (fines, pure coated particles, and agglomerated/coated granules), allowed to identify the main growth mechanisms for an extended range of operating conditions and seed sizes. The agglomeration rate was found to increase by decreasing the fluidization and atomization air flowrates and the bed temperature, as well as by increasing the binder flowrate. The agglomerated mass fraction presented a non-monotonic behavior as a function of the seed diameter, with a minimum at a seed mean diameter of about 0.26 cm. Even though the operating variables were widely disturbed, the main particle growth mechanism was pure coating for all the tested conditions. In fact, coated particles accounted for more than 68 wt.% of the granular product. As a result, the final mass median size remained almost constant for all the studied cases. On the other hand, the span of the particle size distribution was extremely sensitive to the selected operating conditions. This contribution provides some valuable guidelines to avoid agglomeration in melt granulation processes designed to produce coated granules.

1. Introduction

Among the processes handling particulate systems, granulation is a widely-used unit operation for particle enlargement. Granulation allows the production of granules with well-defined particle size distributions and shapes for many industries such as pharmaceutical, agrochemical, detergent, and food industries, among others [1,2].

Typically, three components are needed to produce granules: initial seeds or nuclei, mixing, and a binder. The seeds are always agitated in order to achieve a good binder distribution. Depending on the mixing principle, granulators are often classified into mechanical (e.g., pans, drums, high shear granulators) or pneumatic (fluidized-bed granulators) agitated units [3]. Fluidized-bed granulators (FBG) offer some advantages with respect to other granulation systems, such as the simultaneous spraying, granulation, drying and/or cooling stages, and control, within certain limits, of the granule physical properties by manipulation of some operating variables [4].

Granulation processes are usually also classified according to the binder nature as: wet, dry or melt. In wet granulation, the liquid binder (a solution or dispersion) is distributed on the seeds and, subsequently, the granules are dried to evaporate the solvent. In dry granulation, fine solid particles are added to the agitated seed bed and the powder adherence is promoted by Van der Waals or electrostatic forces [5]. In melt granulation, powders are enlarged by using meltable materials. These last binders are added to the systems either as: 1) powders that melt during the granulation process or 2) atomized molten liquids [6]. The first melt granulation technique is usually called co-melt or *in situ* melt granulation [7], while the second method could be referred as spray-on melt granulation [8]. Certainly, co-melt granulation is not applicable to those systems in which seeds and binder have similar melting temperatures.

In the past, wet granulation has been widely used. Therefore, the number of articles related to wet granulation processes is quite large.

* Corresponding author.
E-mail address: vbucala@plapiqui.edu.ar (V. Bucalá).

http://dx.doi.org/10.1016/j.powtec.2015.09.006
0032-5910/

In the particular case of FBGs, Smith and Nienow [9], Pont et al. [10] and Hemati et al. [11], among others, studied the influence of process variables and seeds/binders physicochemical properties on particle growth kinetics when aqueous solutions were sprayed on beds of solids fluidized by hot air. These experimental studies revealed that many variables affect particle growth mechanism: binder (composition, viscosity, surface tension, flowrate, droplet size) and seed properties (size, shape, porosity), atomization and fluidization air flowrates, nozzle location, bed temperature, etc. Among other variables, the dependence of particle growth regime (agglomeration or coating) and growth rate on excess gas velocity (i.e., the difference between actual and minimum fluidization velocities), was empirically established. For wet granulation and low excess gas velocities, agglomeration was identified as the main particle growth mechanism. For higher gas velocities, the circulation rate of particles increased, thus improving liquid distribution on seed surface and reducing bed quenching by formation of large agglomerates. Moreover, higher gas velocities increased the frequency and energy of inter-particle collisions and particle-wall impacts, breaking the binder solid bridge that may have been formed between primary seeds [9,11]. The same qualitative effect of the fluidization velocity was observed, through experimental work, for different materials and granulator operating variables. However, growth regimes were found to be sensitive to the product and type of granulation unit [8,12,13]. In order to generalize the findings of many authors about wet granulation, the paper published by Ennis et al. [14] was undoubtedly a major turning point. This author proposed a physical-based model for predicting the granules growth behavior. Even though this model is simple and based on many assumptions, it is still helpful to predict growth regimes using measurable variables.

Nowadays, research in melt granulation has become of interest for many applications. This process is considered a more attractive strategy than wet granulation for those materials that are incompatible with water; completely avoiding the use of solvents and the disadvantages associated with solvent recovery and final disposal, and minimizing the energy cost related to solvent evaporation [7,15].

Depending on granules requirements, either agglomeration or coating may be preferred; therefore, understanding the mechanisms prevailing in the granulation process is a prerequisite for obtaining proper control over product properties [16]. Unfortunately, the theories developed for wet granulation are not fully appropriate for describing fluidized-bed melt granulation (FBMG). Consequently, many authors have focused on revealing the influence of some of the most important experimental variables on product quality.

For co-melt granulation, Zhai et al. [6,17] together with Walker et al. [7,18,19] explored the effect of granulation time, binder/granule mass ratio, binder viscosity, and size of the seeds on the granule final size and growth mechanisms. Additionally, Mangwandi et al. [20] investigated the effects of fluidization air velocity, fluidization air temperature and granulation time on granule size, particle size distribution, granule homogeneity and strength.

With regard to spray-on melt granulation, Abberger et al. [15], Boerefijn and Hounslow [16], Seo et al. [21] and Tan et al. [22] studied the effects of binder spray rate, droplet size, seed size, bed temperature, atomization air pressure and fluidization air velocity on the performance of fluidized-bed melt granulation. The studies mainly consisted in *in situ* or top spray-on melt granulation based on polyethylene glycol (PEG) or Poloxamer (either melted or as solid particles) as model binder and glass ballotini or lactose as seeds. In addition, all these processes involved seeds of a very small size, mostly from 0.003 to 0.035 cm. Moreover, for spray-on systems, seed sizes were similar to or even smaller than the sprayed binder droplets. Therefore, particles grew preferentially by agglomeration, being the growth by pure coating insignificant. Even though the conclusions of these studies provide valuable insights into the field of melt granulation, they cannot be applied straightforward to the production of relative big granules through coating.

It is important to note that the granulation process is considered as one of the most significant breakthroughs in the fertilizer industry, providing products with higher resistance and lower tendency for caking and lump formation. In particular, granular urea is the most widely consumed nitrogen-based fertilizer, being critical in the modern agriculture scenario [23]. Industrial urea granulation is mainly performed in fluidized beds [2], which use a highly concentrated urea solution as binder (basically molten urea) sprayed from the bottom. Urea seeds are quite large (about 0.2 cm) and, for some technologies, the binder droplets are significantly smaller than the initial nuclei. Due to the high industrial production rates, high urea melt to seed mass ratios are required (about 50%). In the industrial practice, short granulation times are used and coating is the preferred size enlargement mechanism [24–26].

Based on microscopic observations, Chua et al. [27–29] estimated the time scale of granule–granule collision, droplet–granule collision, and droplet spreading in fluidized-bed melt granulation. They found that the relative importance of these characteristic times had an effect on particle growth mechanisms. However, many of the variables involved in the different time scales came from simulations carried out using computational fluid dynamics (CFD), which allowed to obtain droplet and particle trajectories and velocities; or microscopic determinations such as liquid–solid contact angles, restitution coefficients, instantaneous droplet and particle temperature, etc. The determination of these characteristics times and microscopic parameters is important for establishing the kinetics of the different growth mechanisms (i.e., agglomeration, coating, breakage) required to solve the population balance equation together with the mass and energy balances, in order to predict the product particle size distribution.

This paper is rather focused on the analysis of experimental data from a macroscale point of view, with the purpose of elucidating the effect of the main operating variables on growth mechanism and product quality. This approach is selected, as a first step, because industrial urea granulators are mainly operated by trial and error, being undesired shutdowns quite common and frequent due to big lump formation and out-of-specification final product [30]. Granulation upsets cause important production losses; therefore, macroscopic studies about the influence of operating conditions on growth mechanisms can be useful to make quick decisions in the operation of large-scale urea facilities.

Summarizing, it is the aim of this paper to contribute to a better understanding of the melt granulation process in fluidized beds by varying operating conditions and seed properties in ranges different from those previously reported (i.e., relatively large seed particles compared to the size of the droplets, high binder/seed mass ratios and bottom spray FBMG). The present work deals with a urea (seeds)–urea (binder) system in an attempt to study the impact of seed size, bed temperature, binder flowrate, and fluidization and atomization air flowrates on process parameters (mass balance closure, fines deposited on granulator walls, and granulation efficiency) as well as on product properties (among others, particle size distribution, percentage of particles effectively coated or agglomerated and granule crushing strength) in order to distinguish the operating regions to avoid lump formation or production of granules with low crushing strength. Particularly, in this work growth mechanisms are elucidated by the analysis of the final mass fractions of pure coated particles, agglomerated/coated granules and fine particles.

2. Particle size change mechanisms in fluidized-bed melt granulation

Tan and co-workers [31–33] and Chua et al. [27] reported possible growth and breakage mechanisms that can occur during fluidized-bed melt granulation. Based on the acknowledged feasible growth mechanisms and the observed experimental evidences for urea granulation, Fig. 1 shows a scheme of the microscopic events that can occur during the process (considering that urea is sprayed at around its melting temperature, 132 °C, and the bed is maintained at approximately 100 °C

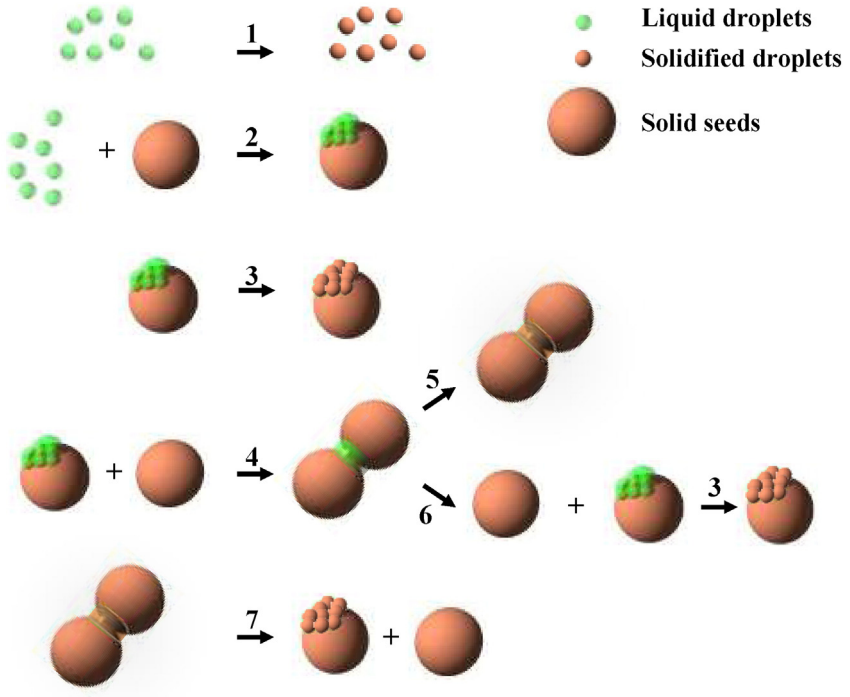

Fig. 1. Schematic of probable microscopic events occurring during urea melt granulation.

[2]). It is worth to remark that the seeds are about 40 times bigger than the urea melt droplets; therefore, Fig. 1 is not representative of the true particles/droplets scale. Some of the smallest droplets may be not captured by the seeds and, thus, be rapidly converted to fine powder (event 1), which could be entrained or recaptured by the solids bed. Event 2 corresponds to the droplet–particle collision; as it can be seen, the liquid binder on the seed surface could either solidify before any other granule touches the wet one (event 3) or get in contact with another particle (event 4). The agglomeration could be successful (event 5) or, depending on the binder solidification rate, the liquid bridge could break (event 6). Finally, and according to the fluidized-bed turbulence, agglomerated particles could be separated through event 7. For the production of urea granules, path 3 is clearly the desired growth mechanism. In order to avoid an exponential granule growth (agglomeration, i.e., event 5 of Fig. 1) and an eventual bed defluidization (known as bed quenching), the operating variables have to be carefully selected.

3. Materials and methods

3.1. Equipment

A schematic diagram of the experimental device is shown in Fig. 2. The experiments were carried out in a batch fluidized-bed granulator constituted by a stainless steel bottom conical vessel (1), which is inclined 6° with respect to the vertical axis (see Table 1), and a cylindrical column (6) on top of it. The air distributor is a stainless steel perforated

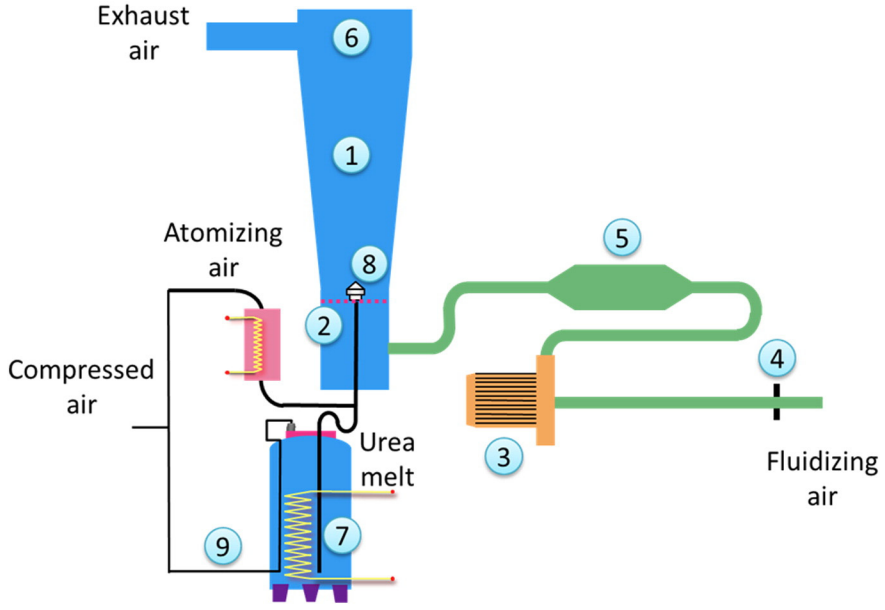

Fig. 2. Schematic representation of the experimental set-up.

Table 1
Granulator geometrical parameters and material properties.

Description	Symbol	Value
Geometrical Parameters		
Conical section height (cm)	H_{co}	70
Cylindrical section height (cm)	H_{cy}	45
Bottom diameter (cm)	D_{bot}	15
Top diameter (cm)	D_{top}	30
Angle (°)	γ	6
Urea		
Solid density (g/cm^3)	ρ_p	1.33
Melt density at 122 °C (g/cm^3)	ρ_l	1.21
Melting temperature (°C)	T_{melt}	132
Air (standard conditions)		
Density (g/cm^3)	ρ_a	$1.20 \cdot 10^{-3}$
Viscosity (poise)	μ_a	$1.81 \cdot 10^{-4}$

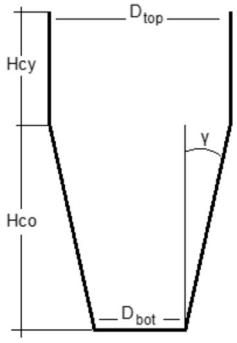

plate (2) of 0.3 cm thick with a porosity of 6% (156 holes, 0.3 cm each hole diameter), covered by an ASTM #30 mesh stainless steel screen in order to prevent solid particles from flowing back into the space below the distributor. The fluidization air was supplied by a centrifugal blower (3). Before entering the bed, the fluidization air flowrate was measured by an orifice flow-meter (4) and preheated by an electrical heater (9 kW) (5) to maintain the bed temperature at the desired level. The bed and grid pressure drops were continuously measured by differential pressure instruments or, alternatively, manually by water U-tube manometers. The elutriated fine particles were collected by a set of three filter bags located at the top of the fluidized-bed freeboard (6). These filters were periodically blown back by air pulses to disengage the particulate matter. The feed (urea melt) was prepared in an oil-heated tank (7) by typically adding 1000 g of urea, a very small volume of water to reach the desired high urea concentration (usually about 97 wt.%) and a tiny amount of food dye to easily monitor the fluidized-bed granulation through the unit observation window. The urea melt tank was placed on a scale and kept at constant temperature ($\approx$130 °C). The urea melt was delivered to an internal mixing two-fluid spray nozzle (8), which was located just above the air distributor, by means of a given compressed air flowrate that was preheated up to 130 °C in an oil reservoir before entering into the urea solution tank (9). The atomization air was also preheated and its flowrate was controlled and measured by a valve and a rotameter, respectively. The external tube-skin temperature of the urea line (from the hot container to the spray nozzle) was controlled through an electric heat tracing system. A Programmable Logic Control system (PLC) was used to register and control several process variables.

3.2. Experimental procedure

For each run, a batch of approximately 2000 g of urea seeds (M_{u_o}) with a given size was initially charged into the bed chamber. The seed size distributions were narrow and obtained by sieving commercial urea particles through two contiguous ASTM sieves with a $2^{1/4}$ geometric ratio (for further details, see Table 3). The seeds were fluidized with hot air until the desired bed temperature level was achieved. Then, the urea melt was sprayed at a constant mass flowrate. This flowrate was computed from the linear time profile of the recorded urea container weight. Once the binder spraying was stopped, the granules were immediately cooled down using air at room temperature. The collected granular product (M_{u_f}) was set aside for further characterization. After each experiment, the powder deposited onto the granulator walls and the fines collected in the filter bags were weighted for mass balance closure calculations. Several experiments were performed to understand the effects of different operating variables on the growth mechanisms, granulation efficiency and granule final properties. To this end and as it can be seen in Table 2, the superficial fluidization air velocity (v_f) at standard conditions was varied from 217.8 to 446.3 cm/s, the arithmetic mass mean diameter of the urea seeds (d_0) from 0.155 to 0.368 cm (see also Table 3), the urea melt flowrate ($\dot{M}_{melt}$) from 4.5 to 17.4 g/s, the bed temperature set-point (T_{bed}) from 90 to 110 °C and the atomization air flowrate ($\dot{Q}_a$) from 417 to 667 cm^3/s.

3.3. Granular product and process characterization

3.3.1. Droplet sizes

No direct measurements of droplet sizes were performed. For some representative experiments, the melt was sprayed in an empty bed and the product fines analyzed by laser diffraction (Laser Diffraction Particle Size Analyzer LA-950, HORIBA). The mass median of the fines was always below 59 μm. Assuming that: a) each particle of the fines was generated by a single spherical droplet of the same urea mass, b) the melt and solid densities reported in Table 1 and c) considering an average urea content $X_u = 0.97$, the mass median of the droplet diameter was expected to be lower than 61.5 μm. Hence, the seeds were at least about 40 times bigger than the expected droplet size.

3.3.2. Particle size distributions

The particle size distributions (PSDs) were evaluated for the solids collected at the end of the experiments (i.e., final granular product). A riffle splitter was used to accurately divide the total sample (about 3000 g) into representative samples. A batch of 800 g was sieved in a vibratory sieve shaker (Zonytest, Argentina). A series of nine ASTM standard sieves (#4, 5, 6, 7, 8, 10, 12, 14 and 16) was employed. The sample was shaken for 20 min at about 2400 strokes per minute.

3.3.3. Representative sizes

To analyze the final product granulometry, the representative sizes d_{10}, d_{50} (median mass size) and d_{90} were calculated from the normalized cumulative mass passing distributions. d_{10}, d_{50} and d_{90} represent the opening sizes that would let pass 10, 50 and 90 wt.% of the sample, respectively.

3.3.4. Process fines mass fractions and mass balance closure

Fig. 3 shows a schematic of the urea mass balance at the end of the experiments. The process fines (i.e., fines not collected within the granular product) were grouped into the following two categories:

- *Wall fines mass fraction* (F_w): represents the mass percentage of total powder deposited onto the granulator walls with respect to the sprayed urea.

Table 2
Operating conditions.

Variable	Symbol	Base case	Case I	Case II	Case III	Case IV	Case V	Case VI
Urea flowrate (g/s)	$\dot{M}_{melt}$	4.6	5.0–16.5	4.0–17.4	4.6 ± 5.6%	4.6 ± 5.9%	4.6 ± 5.5%	4.5 ± 5.7%
Fluidization air velocity* (cm/s)	v_f	300	395.0 ± 1.6%	305.7 ± 1.4%	217.8–446.3	297.8 ± 3.0%	301.2 ± 1.8%	302.7 ± 1.9%
Atomization air flowrate# (cm^3/s)	$\dot{Q}_a$	500	500	500	500	417.0–666.7	500	500
Seed arithmetic mean diameter (10^{-1}cm)	d_0	2.59	2.59	2.59	2.59	2.59	1.55–3.68	2.59
Bed temperature set point (°C)	T_{bed}	100	100	100	100	100	100	90–110
Feed urea concentration (wt.%)	X_u	97	97.3 ± 0.5%	96.9 ± 0.3%	96.3 ± 0.4%	96.5 ± 0.4%	96.3 ± 0.4%	96.6 ± 0.4%
Initial mass (g)	M_{u0}	2000	2000	2000	2000	2000	2000	2000
Maximum sprayed urea mass (g)	M_{us}	1000	1000	1000	1000	1000	1000	1000

* At standard conditions.
\# At 130 °C and 3 bars.

- *Filter-bags fines mass fraction* (F_f): represents the mass percentage of powder retained in the filters with respect to the sprayed urea.

To perform the mass balance closure, the granulation efficiency was defined as:

$$\eta = \frac{M_{uf} - M_{u0}}{\dot{M}_{melt} X_u t}.100 \quad (1)$$

where t and X_u represent the total duration of the urea spraying and the binder urea content, respectively.

Therefore, the total mass balance was given by:

$$100 = F_f + F_w + F_{lost} + \eta \quad (2)$$

where F_{lost} represents the mass percentage of lost urea with respect to the total sprayed urea, and was calculated from Eq. (2).

3.3.5. Granular product size fractions

According to Fig. 3, the final granular product was represented by three mass fractions:

- *Product fines mass fraction* (F_p)*:* represents the mass percentage of particles smaller than the seeds with respect to the total final granular product. Laser diffraction analysis of the collected product fines (base case) revealed that their sizes were between 32 and 75 μm; i.e. very fine powder.
- *Product agglomerated mass fraction* (A)*:* represents the mass percentage of agglomerated particles with respect to the final mass of granular product. When agglomeration took place, the total mass retained on some sieves corresponded to agglomerated particles while other meshes retained both, pure coated particles and small agglomerates. For these cases, a riffle splitter was used to subdivide the retained mass, and the agglomerates were recognized by visual inspection and quantified by weighting.
- *Product pure coated mass fraction* (C)*:* denotes the mass percentage of pure coated particles, and was calculated as follows:

$$C = 100 - A - F_p. \quad (3)$$

3.3.6. Granule moisture content

Representative granule samples of 10 g (immediately collected after each granulation run) were dried at 95 °C for 9 min in an Ohaus MB45 moisture analyzer. This treatment profile was defined, using some selected samples, to reproduce the moisture content measured by the Karl–Fisher method. The moisture content was determined in triplicates.

3.3.7. Granule crushing strength

A testing machine Instron model 3369 in compression mode at a speed of 2 mm/min was used. For each experiment the crushing strength, which is affected by the granule size, was measured for the product particles that were trapped in the upper mesh of the seed size range to ensure the evaluation of equal-size granules. For example and according to Table 3, when seeds between ASTM meshes #7 and #8 were selected, the tested granules were the ones trapped in the apertures of mesh #7. For each sample, twenty measurements were performed.

3.3.8. Particle morphology

The morphology of the external surface and cross-sectional cuts of some selected granules were assessed in an EVO 40-XVP, LEO Scanning Electron Microscope (SEM). The samples were previously metalized with gold in a PELCO 91000 sputter coater.

4. Population balance equation for pure coating growth mechanism

An appropriate modeling approach to predict PSDs is the concept of population balance equation (PBE), which was developed several decades ago [34]. Significant efforts were those of Randolph and Larson [35] and Ramkrishna [36] to formalize a generic PBE by quantifying the different mechanisms by which the particle sizes can change. In general, the PBE has no analytical solution; therefore, numerical methods are required for precise calculation of the PSDs. However, for a perfectly-mixed batch granulator wherein the only particle size change mechanism is coating, the PBE can be described as a parameterized equation [36,37]:

$$\frac{dF'}{dt} = 0 \quad (4)$$

Table 3
Case V: Seed sizes.

Case	ASTM lower mesh	ASTM upper mesh	Lower aperture, cm	Upper aperture, cm	d_0, cm
V.1	6	5	$3.36 \cdot 10^{-1}$	$4.00 \cdot 10^{-1}$	$3.68 \cdot 10^{-1}$
V.2	7	6	$2.80 \cdot 10^{-1}$	$3.36 \cdot 10^{-1}$	$3.08 \cdot 10^{-1}$
V.3	8	7	$2.38 \cdot 10^{-1}$	$2.80 \cdot 10^{-1}$	$2.59 \cdot 10^{-1}$
V.4	10	8	$2.00 \cdot 10^{-1}$	$2.38 \cdot 10^{-1}$	$2.19 \cdot 10^{-1}$
V.5	12	10	$1.68 \cdot 10^{-1}$	$2.00 \cdot 10^{-1}$	$1.84 \cdot 10^{-1}$
V.6	14	12	$1.41 \cdot 10^{-1}$	$1.68 \cdot 10^{-1}$	$1.55 \cdot 10^{-1}$

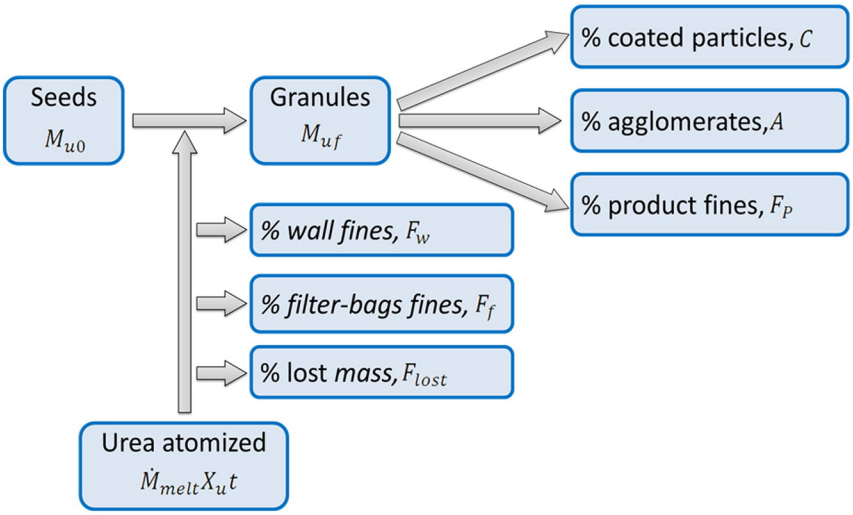

Fig. 3. Urea mass balance at the end of the experiments.

$$\frac{dd}{dt} = G \tag{5}$$

where F' and d represent the normalized cumulative number passing function and the particle diameter along the characteristic curve, respectively. G is the coating growth rate, i.e., the rate at which the particles grow by coating. The growth rate is usually assumed independent of the particle sizes and is expressed as follows [5]:

$$G = \eta \frac{2\dot{M}_{melt} X_u}{\rho_p A_T} \tag{6}$$

where A_T is the particles total external surface area and, as aforementioned, $\dot{M}_{melt}$ is the urea melt flowrate and X_u is the binder urea content. Due to the granules growth, A_T increases as coating takes place; therefore, G becomes time dependent. By replacing Eq. (6) in Eq. (5), the following equation can be used to predict the particle size distribution as granulation proceeds:

$$d_i'(t) = d_i'(0) + \int_0^t \eta \frac{2\dot{M}_{melt} X_u}{\rho_p A_T} dt \tag{7}$$

On the other hand, the solution of Eq. (4) leads to:

$$F_i'(t) = F_i'(0) \tag{8}$$

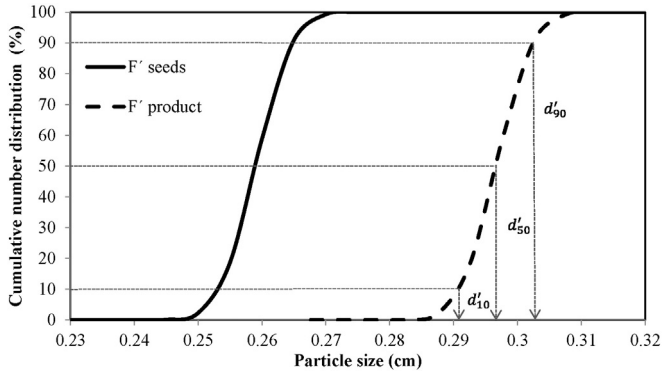

Fig. 4. Normalized cumulative number passing distribution (F') for seeds and granular product as a function of the particle size.

Eqs. (7) and (8) represent the PBE solution, which indicates that the granular product number PSD is defined by the seed PSD shifted to larger particle diameters (Eq. (7)) [36,38]. Fig. 4 schematically shows the number PSD evolution.

In the present work, the thickness of the coating layer was very low compared to the seed size; therefore, the total external area of the particles can be assumed constant during the experiments and equal to the initial one. Then, Eq. (7) can be rewritten as:

$$d_i'(t) = d_i'(0) + \eta \frac{2\dot{M}_{melt} X_u t}{\rho_p A_{T_0}}. \tag{9}$$

The initial external area of the particles A_{T_0} is given by:

$$A_{T_0} = N_0 \, \pi \bar{d}_{SN_0}{}^2 \tag{10}$$

where $\bar{d}_{SN_0}$ is the mean surface-number diameter and N_0 represents the total number of seeds. N_0 can be calculated through the following equation:

$$N_0 = \frac{6\, M_{u0}}{\rho_p \, \pi \bar{d}_{NV_0}{}^3} \tag{11}$$

where $\bar{d}_{NV_0}$ denotes the seed mean number-volume diameter. Taking into account Eqs. (10) and (11) and that the seed PSD is very narrow (i.e., $\bar{d}_{NV_0} \approx \bar{d}_{SN_0} \approx d_0$), Eq. (9) becomes:

$$d_i'(t) = d_i'(0) + d_0 \, \eta \frac{\dot{M}_{melt} X_u t}{3\, M_{u0}}. \tag{12}$$

If the class i is named by its F_i' value, Eq. (12) can be used to calculate the representative diameters of a number PSD:

$$d'_{10}(t) = d'_{10}(0) + d_0 \, \eta \frac{\dot{M}_{melt} X_u t}{3\, M_{u0}} \tag{13}$$

$$d'_{50}(t) = d'_{50}(0) + d_0 \, \eta \frac{\dot{M}_{melt} X_u t}{3\, M_{u0}} \tag{14}$$

$$d'_{90}(t) = d'_{90}(0) + d_0 \, \eta \frac{\dot{M}_{melt} X_u t}{3\, M_{u0}}. \tag{15}$$

It was proved (data not shown) that for the experimental growth rates (lower than 0.04 cm/s), the normalized cumulative number

passing distributions were very similar to the normalized cumulative mass passing PSDs. Therefore, Eqs. (13)–(15) can also be applied to calculate the representative diameters for mass PSDs (i.e., d_{10}, d_{50} and d_{90}), which will be used to discuss the experimental results.

5. Results and discussions

Based on the experimental results, a base case of high granulation efficiency and granules growth by pure coating was selected. The process conditions for this base case are listed in Table 2. These conditions were disturbed to study the effect of the binder flowrate (Cases I and II), fluidization air flowrate (Case III), atomization air flowrate (Case IV), seed size (Case V) and bed temperature (Case VI) on process parameters and product properties. For each study case, all the remaining process conditions were kept constant at their base case values.

5.1. Effect of melt flowrate

For two levels of fluidization air velocity (400 cm/s: Case I and 300 cm/s: Case II), the influence of the melt flowrate on the granulation process was studied.

Fig. 5 shows, for Case I, the granulation efficiency together with the wall and filter-bags fines mass fractions. For this case, the mass lost during the experiments was in average 2.8 wt.%, value that indicates a good mass balance closure. Considering that F_{lost} was nearly constant for all the experiments, Eq. (2) indicates that a decrease in the granulation efficiency due to an increase in the binder flowrate should be accompanied by an increase in the process fines mass fractions, as shown in Fig. 4. The filter-bags fines were substantially higher than the ones collected from the granulation chamber wall. However, for melt flowrates varying between 5 and 17 g/s, the mass fraction $\frac{F_f}{F_w}$ changed from 13 to 3, respectively. This result indicates that the wall fines (F_w) increased at a rate higher than the elutriated ones (F_f). The amount of molten liquid on the particle surface is expected to increase for higher melt flowrates; therefore, the solidification time should increase. Under these conditions, the particles may collide with the chamber wall when they are still wet, increasing the probability of material adhesion on the unit wall. It is also observed that the higher the melt flowrate the higher the filter-bags fines; this behavior indicates that a higher mass fraction of solidified droplets (event 1, Fig. 1) was elutriated out of the granulator.

Changes on the fluidization velocity from 400 to 300 cm/s gave the same trends for the variables shown in Fig. 5. However, for 300 cm/s (data not shown) the wall fines were higher compared to those found for 400 cm/s, result that is in good agreement with the fact that the lower the air velocity the lower the solidification rate, and therefore the higher the probability of wet material adhesion on the granulation chamber walls.

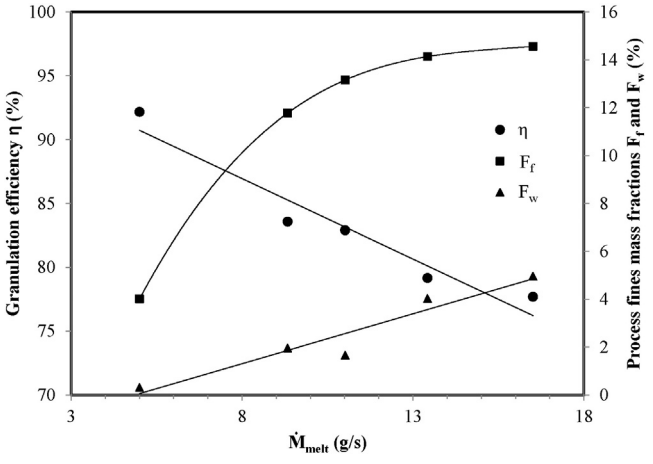

Fig. 5. Case I. Granulation efficiency and process fines mass fractions as a function of the binder flowrate.

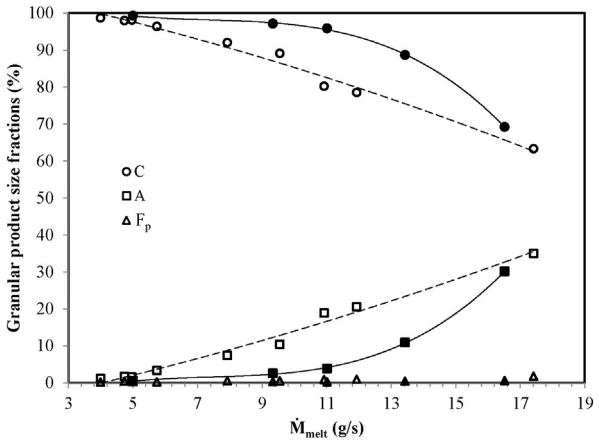

Fig. 6. Cases I and II. Granular product size fractions as a function of the binder flowrate (solid points: 400 cm/s; open points: 300 cm/s).

For Cases I and II, the granular product size fractions as a function of the melt flowrate are shown in Fig. 6. For the explored conditions, the product fines mass fractions were negligible, representing less than 2 wt.% of the total granular product. For a constant fluidization velocity, as the binder flowrate increased, the interparticle interactions by formation of liquid bridges were favored leading to higher agglomerate mass fractions (events 4 and 5, Fig. 1). Consequently, the fraction of pure coated particles decreased. The product characterization (C, A and F_p mass fractions) according to the size enlargement process, allows identifying the operating conditions for which pure coating evolves to a combined coating/agglomeration growth mechanism. Comparing Cases I and II, it is clear that this transition occurred at higher melt flowrates when higher fluidization velocities were used.

Fig. 7 presents mass fraction histograms for the seeds and some representative granular products (Case I at two different melt mass flowrates). Besides, some granule pictures are included to illustrate the qualitative aspect of the different cut sizes. According to Fig. 6, for Case I with a binder flowrate of 5 g/s, pure coating took place. Considering that: a) the seeds belonged to the size class 0.238–0.28 cm, b) the experimental granulation efficiency was around 92% (see Fig. 5) and c) the hypothesis of a perfectly-mixed granulator, Eq. (12) allows establishing that the final granule size range should be 0.27–0.32 cm. Experimentally, 86% of the total mass of the granular product was distributed between the size ranges 0.238–0.28 and 0.28–0.336 cm, and only the remaining 14% corresponded to 0.336–0.4 cm. This result indicates that there was not a very significant deviation of the granulator flow pattern with respect to the perfect mixing model. On the other hand, for a melt flowrate of 16.5 g/s, Fig. 6 indicates that the agglomerates accounted for 30% of the total product mass. Consequently, the total particle number decreased with respect to the initial seed number; for this case, Eq. (12) is not valid and therefore the final product size range cannot be easily predicted. In fact, the particle size distribution for a melt flowrate of 16.5 g/s was wider than the one corresponding to 5 g/s. The pictures included in Fig. 7 show that for the highest melt flowrate, particles grew by a combined agglomeration-coating process for sizes higher than 0.336 cm. Nevertheless, for both melt flowrates, high mass fractions (higher or equal to 50%) of pure coated particles within the size range 0.28–0.336 cm (mean size of 0.31 cm) were observed.

To compare the particle size distributions for all the tested binder flowrates and fluidization velocities (Cases I and II), Fig. 8 shows the d_{10}, d_{50} and d_{90} sizes obtained from the sieving data. Even though different growth mechanisms took place, for all the melt flowrates and

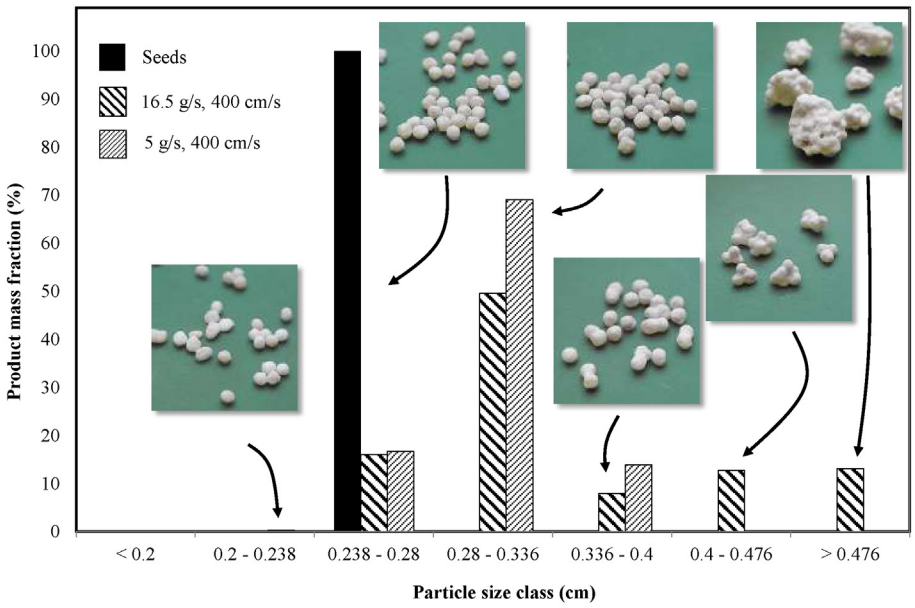

Fig. 7. Case I. Mass fraction histograms for different binder flowrates.

fluidization velocities, d_{10} and d_{50} were almost constant and close to 0.27 and 0.31 cm, respectively. However, when agglomeration became an important growth mechanism, d_{90} was strongly affected by both the binder mass flowrate and fluidization velocity.

Considering agglomeration as the main growth mechanism and for a constant ratio between the added binder and seed mass, Tan et al. [22] observed that the population mean diameter was not affected by the binder flowrate. The findings of this contribution are then in good agreement with the results previously reported, even when not only agglomeration takes place and for seed/droplet size ratios much larger than those used by Tan et al. [22]. It is very important to point out that for systems where either pure coating or combined coating/agglomeration may occur, as the one studied in this work, the mean diameter (e.g. d_{50}) does not allow concluding the prevalence of any growth mechanisms. Although the melt flowrate did not affect the population mean size, it significantly influenced the growth mechanisms even for a constant binder/seed mass ratio.

In order to describe the granulator fluidization dynamics, Fig. 9 shows the ratio between the fluidization (v_f) and the minimum fluidization (v_{mf}) velocities for different representative particle sizes. The constant lines represent the relationships between the fluidization velocities used in this analysis (i.e., 300 and 400 cm/s) and the experimental v_{mf} measured in the fluidized bed when it was loaded with seeds of 0.259 cm. For each studied binder flowrate, Fig. 9 also displays the relationships $(v_f/v_{mf})|_{d_{50}}$ and $(v_f/v_{mf})|_{d_{90}}$. The characteristic sizes d_{50} and d_{90} were estimated from the experimental sieving data of the granular product, while the corresponding v_{mf} were calculated values [1]. As it can be seen in Fig. 9, the selected fluidization velocities were about 4.8 and 3.6 times the v_{mf} measured for the seeds, indicating good fluidization at the beginning of the experiments. For particles sizes equal to d_{50}, the fluidization velocities of 300 and 400 cm/s were about 3 and 4.2 times bigger than the corresponding v_{mf}, respectively. As the binder flowrate increased, the $(v_f/v_{mf})|_{d_{90}}$ ratio decreased significantly. Particularly, for 300 cm/s the $(v_f/v_{mf})|_{d_{90}}$ ratio became equal to 1 for high melt flowrates. This result indicates poor fluidization conditions, which may contribute to the increase in the agglomeration rates with respect the coating ones.

Regarding the coated granules properties, Fig. 10 shows the particle moisture content and crushing strength as a function of the melt flowrate. For a constant fluidization air velocity (e.g., 400 cm/s), the moisture content increased with the binder flowrate (for a fixed X_u, the higher the binder flowrate, the higher the water loading). In agreement with the results reported by Walker et al. [39], the fertilizer

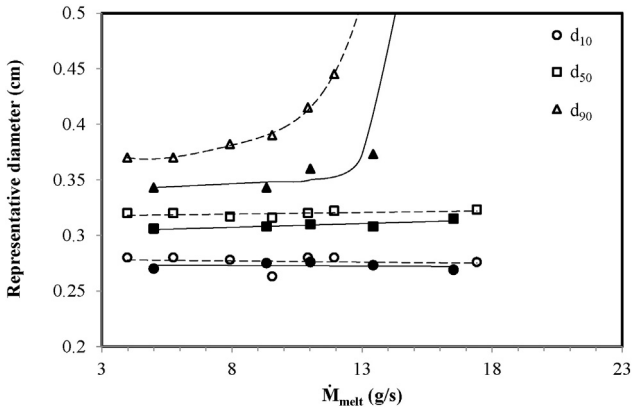

Fig. 8. Cases I and II. Representative diameters as a function of $\dot{M}_{melt}$ (solid points: 400 cm/s, open points: 300 cm/s).

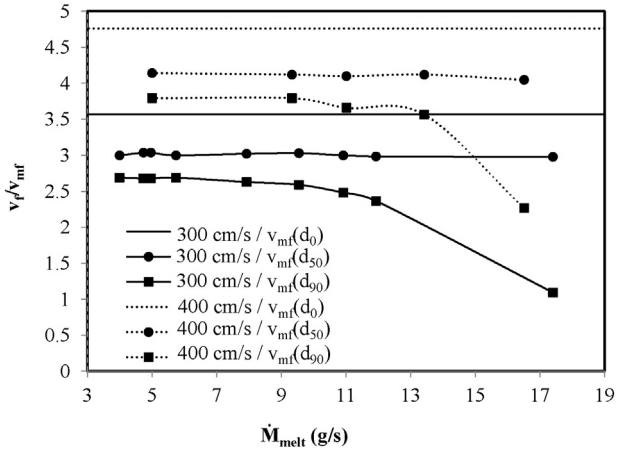

Fig. 9. Cases I and II. Fluidization velocity to minimum fluidization velocity ratio for different particle diameters as a function of the binder flowrate.

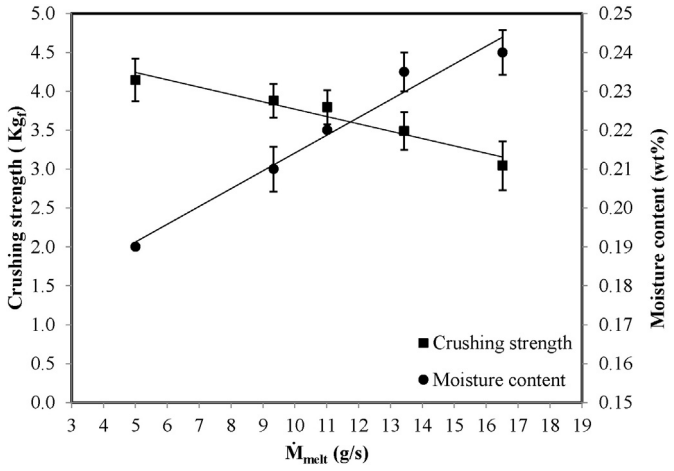

Fig. 10. Case I. Moisture content and crushing strength as a function of the binder flowrate.

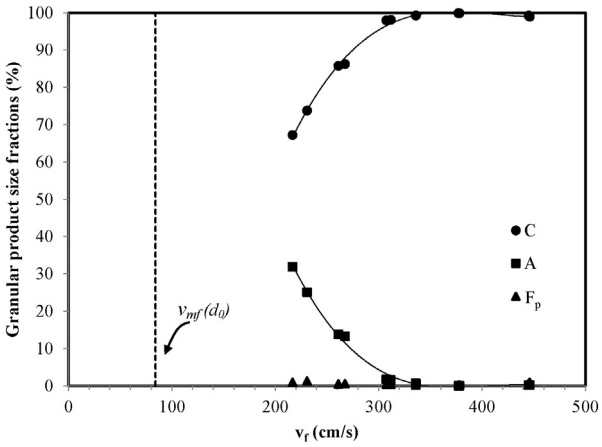

Fig. 12. Case III. Granular product size fractions as a function of the fluidization air velocity.

granules with higher water contents exhibited lower crushing strengths. Nevertheless, the coated particles fulfilled the fertilizer granule requirements (i.e., moisture content lower than 0.5 wt.% and crushing strengths higher than 1.5 kg_f [40]).

Concerning the granules morphology, Fig. 11 presents SEM micrographs for Case II and a binder flowrate of 10.9 g/s. Fig. 11a shows a rounded coated particle with a mean size of 0.298 cm, while Fig. 11b depicts the cross-sectional morphology of a selected granule. The seeds, which are the core of the coated particles, corresponded to industrial granular urea. Considering the seed size of about 0.259 cm and the final granule diameter of 0.298, the expected growth thickness of 190 μm is in good agreement with the mean experimental thickness shown in Fig. 11b (195 μm).

5.2. Effect of fluidization air velocity

The fluidization air velocity was recognized by several authors as a very important operating variable to control the particles growth mechanisms, either for wet [9,11] or melt granulation [22]. For this reason, in this work v_f was approximately modified from 220 to 450 cm/s. The lowest and the highest values were about 2.6 and 5.4 times the seeds' minimum fluidization velocity. The minimum fluidization velocity was experimentally determined by registering the bed pressure drop as a function of the superficial air velocity at the bottom of the conical unit. Through this procedure, a value of 0.82 m/s for v_{mf} was obtained for the base case. Experiments at even lower velocities were also performed; however; bed defluidization was observed for $(v_f/v_{mf})|_{d_0}$ lower than 2.

As for the other cases, the influence of the fluidization air velocity on both the granulation process and product quality was analyzed. The granulation efficiencies were all higher than 87%, being the average value 92%. The maximum F_{lost}, F_f and F_w were 7.4, 5.7 and 2.6%, respectively, being the filter-bags and granulator wall fines of this case (Case III) much lower than the amounts collected in Cases I and II.

Fig. 12 shows the granular product size fractions as a function of the fluidization air velocity. For the explored conditions, the product fines mass fractions were very low, representing less than 1.3 wt.% of the total granular product. For relatively high fluidization air velocities, and in agreement with data reported for other wet or melt granulation systems [9,11] coating appeared as the dominant growth mechanism. In fact, for fluidization velocities higher than 325 cm/s the agglomerate mass fraction was lower than 1%. This fluidization velocity value corresponds to about four times the seeds' minimum fluidization velocity (see Fig. 12). As the fluidization velocity decreases, the agglomerate mass fraction turned noticeable. For the lowest tested fluidization velocity (217 cm/s), Fig. 12 shows that the agglomerate mass fraction corresponded to a maximum value of 32%. It is well known that high fluidization velocities favor the particles movement, which is achieved by the presence of bubbles. The bubbles are strongly related to the excess gas velocity ($v_e = v_f - v_{mf}$), the higher v_e the higher the particle mixing.

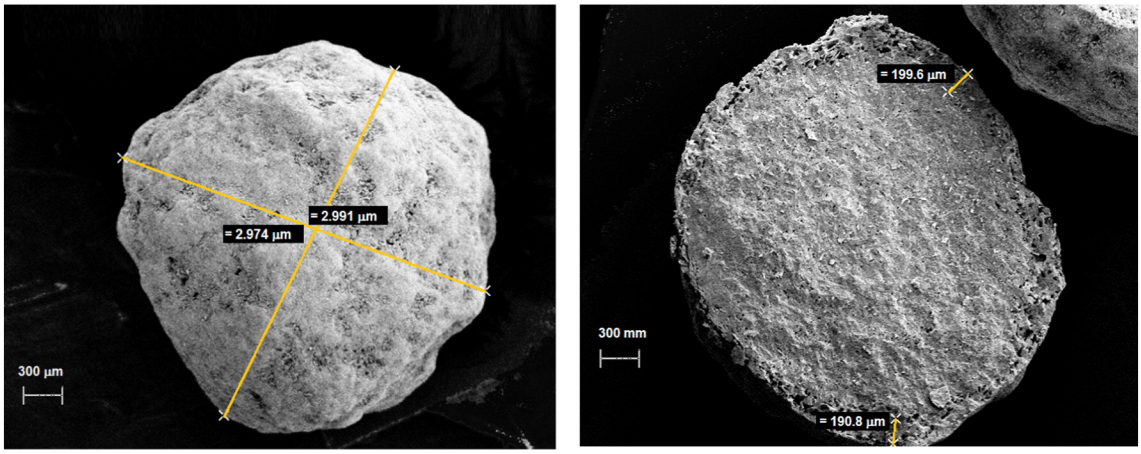

Fig. 11. Case II. SEM micrographs: a) coated granule, b) granule internal surface. $\dot{M}_{melt} = 10.9$ g/s.

When v_e decreases, the fluidization conditions become worse and agglomeration is drastically triggered. Unfortunately, as pointed out by Smith and Nienow [9], agglomeration for different systems takes place at diverse v_f/v_{mf}, being the beginning of this enlargement process dependent of many operating variables and binder and seed properties. In fact, these authors found agglomeration for excess gas velocities lower than 28 cm/s, while in this work even excess gas velocities of 130 cm/s led to agglomerates. This proved that the excess gas velocity (or its dimensionless form v_f/v_{mf}) required to favor coating does not assume the same value for different systems and, therefore, more experimental data are needed to build general theories.

At high fluidization velocities, since the selected binder amount did not fully dissipate the high kinetic energy, pure coating prevailed (event 3, Fig. 1). Also, the higher the air flowrate the higher the heat transfer; therefore, the droplets might have solidified faster avoiding wet particle interactions. Even though wet particles collisions (event 4) could have occurred to some extent, the disruptive forces caused by the high particles motion are expected to detach any eventual particle interaction by breakage of liquid bridges (event 6) or even solid bridges (event 7), and consequently favor event 3.

Fig. 13 shows the histograms for selected experiments of Case III, as well as d_{10}, d_{50} and d_{90} as a function of the fluidization air velocity. d_{10} and d_{50} were almost constant and close to 0.27 and 0.31 cm, respectively; values that are exactly the same as those found for the previously discussed cases (Fig. 8). The histograms for 217 and 378 cm/s indicate that the normalized cumulative mass of particles lower than 0.336 cm accounted for 63% and 84%, respectively. These values reflect that coating is the main enlargement process.

At fluidization air velocities lower than 325 cm/s, d_{90} increased considerably due to the higher agglomerate mass fractions within the product. On the other hand, at high air velocities, where the coating mechanism was dominant, d_{90} remained practically constant and independent of the fluidization flowrate.

Moisture content analyses of coated granules indicate that the water content decreased as the fluidization air velocity increased. These results are in good agreement with the expected heat and mass transfer enhancement for intense mixed systems. For fluidization air velocities varying between 217 and 450 cm/s, the moisture content changed from approximately 0.29 to 0.16 wt.%, respectively. As well as for Cases I and II, the crushing strength exhibited an opposite trend to that observed for the moisture content. The more resistant granules were found for the higher air flowrates (crushing strengths up to 4.8 kg_f were measured). As mentioned by Iveson et al. [12], higher consolidation is expected when the collisions intensity between particles and particles–granulator wall are higher. Nevertheless, for the lowest air velocity the crushing strength was about 3 kg_f, which still is a good value for granular fertilizers [40].

5.3. Effect of atomization air flowrate

The atomization air flowrate was varied from 417 to 670 cm^3/s. As mentioned in Section 3.3.1, the droplet sizes were not directly measured; however; the PSD of the fines obtained in an empty fluidized bed were analyzed. The mass medians were 59, 49 and 25 μm for atomization air flowrates of 417, 583 and 670 cm^3/s, respectively.

The granulation efficiency was higher than 87%, being the average value equal to 89%. All the experiments presented reasonable mass balance closures; in fact, the maximum lost mass was 7.1%. Consistently with Eq. (2), the process fines were very low. Particularly, the wall fines were lower than 2.6%. It is important to note that while the binder flowrate does not strongly affect the droplets size distribution, the atomization flowrate has a significant impact [11]. In fact, noticeable smaller droplets were obtained for higher atomization air flowrates. Then, the observed low F_w values suggest that, despite the change in the droplet size, the drops solidify before the wet particles reach the granulator wall. Even though the atomization rate was changed, the droplet sizes remained small enough to rapidly solidify. Also, as suggested by the granules micrographs (Fig. 11), the atomized droplets should be much smaller than the seeds; therefore, the atomization air flowrate variations should not strongly affect either the seed size/droplet size ratio or the growth mechanism. According to this, Fig. 14 (which displays the product mass fractions as a function of the atomization air flowrate) points out that the mass of agglomerates was lower than 7%, being coating the main particles growth mechanism.

For all the studied atomization flowrates, and as for the previous cases, d_{10} and d_{50} remained almost invariant (data not shown) being the mean values close to 0.27 and 0.31 cm, respectively. On the other hand, d_{90} varied from 0.37 to 0.33 when the air flowrate was changed from 416 to 667 cm/s, respectively. There was a slight decrease in d_{90} as the atomization air flowrate increased because coating became the prevailing growth mechanism.

For all the experiments, the coated granules moisture content was very low, being the mean value around 0.2 wt.%. Regarding the crushing strength, an average value of about of 4 kg_f was found.

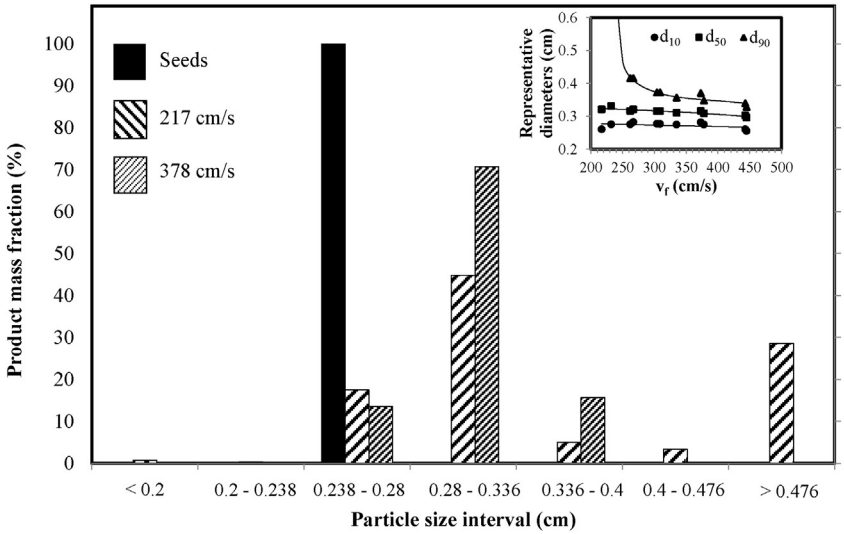

Fig. 13. Case III. Mass fraction histograms for different fluidization air velocities and representative diameters as a function of v_f.

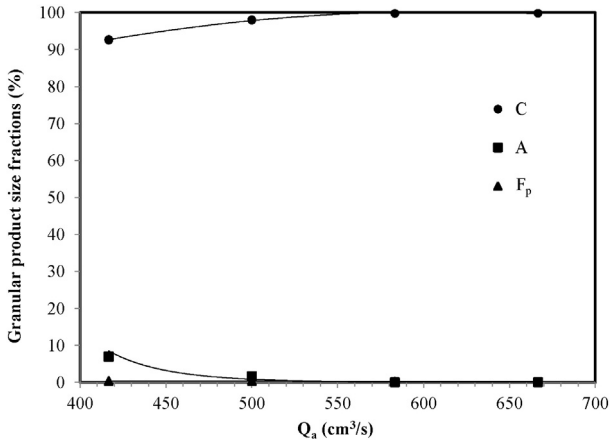

Fig. 14. Case IV. Product mass fractions as a function of the atomization air flowrate.

5.4. Effect of seed sizes

For this case (Case V), F_{lost} was lower than 5%, indicating, once again, a good mass balance closure. The granulation efficiency was higher than 88% for the entire explored seed size ranges. Besides, the granulation efficiency variation with the seed diameter was not significant.

Fig. 15 shows the agglomerate and product fines as a function of the seed diameter. The agglomerate mass fraction was very low, being less than 6% for all the studied seed size ranges. Interestingly, the agglomerates trend presented a non-monotonic behavior, with a minimum value of agglomerates for the seeds with 0.259 cm as mean diameter (base case). Several authors found, for wet granulation, that agglomerate formation decreases as the seed size increases [9,11,41]. This trend is observed in Fig. 15 for the seeds smaller than 0.259 cm. Indeed, the bigger the seeds the higher their kinetic energy, and thus the lower the probability of particles agglomeration (i.e., more energy has to be dissipated by the liquid bridges). In contrast, for the seeds bigger than 0.259 cm, the agglomerate mass fraction increased with the seed size. To explain this behavior, Eq. (12) (valid for a pure coating process) can be used to calculate the thickness of the liquid layer (l):

$$l(t) = \frac{d_i'(t) - d'(0)}{2} = \frac{d_0 \eta \dot{M}_{melt} X_u t}{6 M_{u0}}. \quad (16)$$

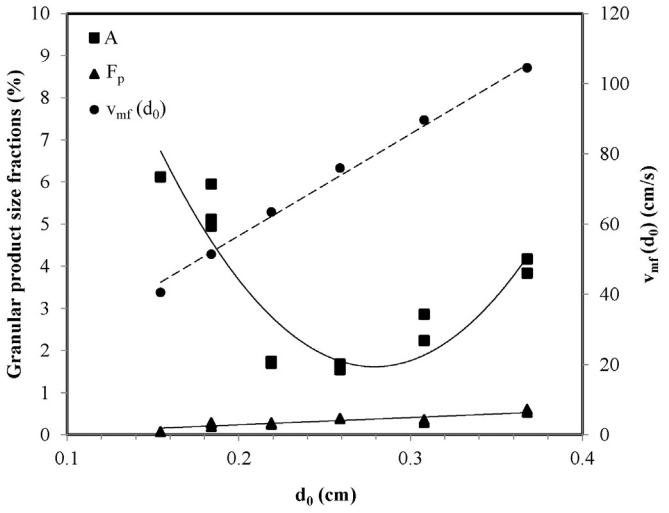

Fig. 15. Case V. Product agglomerates, fines fractions and $v_{mf}(d_0)$ as a function of the seed size.

Considering that the sprayed urea mass and the seed mass were kept constant (Table 2), Eq. (16) indicates that the thickness of the liquid layer deposited on each particle has to be proportional to the seed size. At the end of the experiments and assuming granulation efficiencies of 90%, the liquid thickness for pure coated particles should follow the linear relationship given by $l \approx 0.0655\, d_0$. Then, higher melt solidification times are expected for the thicker liquid layers associated to the bigger seeds. The thicker the liquid layer the higher the probability of seed agglomeration (i.e., more kinetic energy can be absorbed). Even though Eq. (16) is not valid when agglomeration takes place, the liquid layer thickness should also increase with the seed size (the total external area per unit mass is expected to decrease). The trend observed for particles bigger than 0.259 cm is in good agreement with the results reported by Abberger et al. [15] for melt granulation. The agglomeration for particles bigger than 0.259 cm is also reinforced by the fact that the v_f/v_{mf} relationship decreased as the seed size increased (see v_{mf} in Fig. 15).

Fig. 15 also indicates that the fines mass fraction in the granular product was lower than 0.6% for all the experiments, with a slight fines increase for the bigger seeds.

Fig. 16 shows the granular product representative diameters as a function of the seed size. As expected, d_{10}, d_{50} and d_{90} increased with the seed size. In order to provide a reference, a 45° straight line is also included in Fig. 16. For pure coating and constant binder/seed mass ratio, Eq. (12) indicates that the particle size enlargement has to be proportional to the seed mean diameter. Therefore, the representative diameters as a function of d_0 should have identical slopes; any deviation suggests that other mechanisms than pure coating may take place (e.g., nucleation, agglomeration). The slope of the d_{10} straight line is lower than 1, indicating that there were more product fines as the seed size was increased (also see Fig. 15). As it was previously mentioned, the bigger the seeds the lower the total particle external area and, therefore, the lower the amount of droplets that can be captured by the seeds. As a consequence, nucleation may occur (event 1, Fig. 1), increasing the small particles mass fraction within the product. The slope of the d_{90} straight line did not deviate from the expected value, confirming that agglomeration was not very significant (see Fig. 15).

Regarding the granules properties, the seed size did not affect the moisture content, which was nearly constant at 0.2 wt.%. However, and as expected, the crushing strength of the coated particles was higher for the bigger seeds (see Fig. 17). For seeds smaller than 0.336 cm, the crushing strength of the coated particles presented good linearity; relationship previously reported by Walker et al. [39].

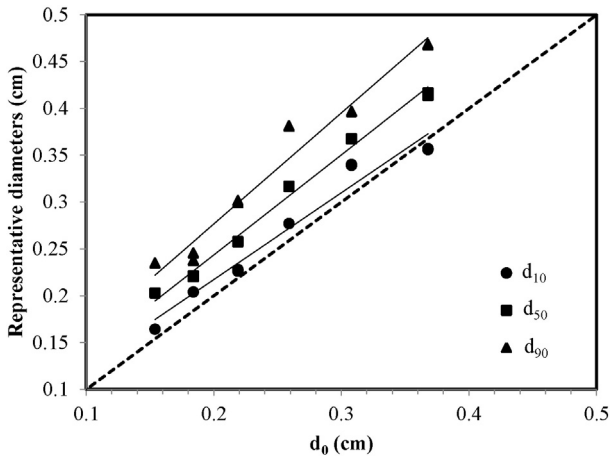

Fig. 16. Case V. Representative diameters as a function of seed size.

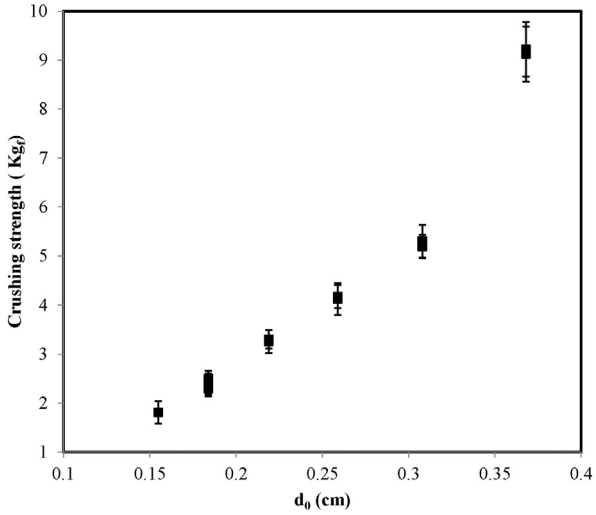

Fig. 17. Case V. Crushing strength as a function of the seed size.

5.5. Effect of bed temperature

The bed temperature was varied from 90 to 110 °C, well below the urea melting point (132 °C). For this case, the granulation efficiency was higher than 87%, the mass lost fraction was lower than 5% and the process fines accounted for, as maximum, 8%. Therefore, the bed temperature did not noticeably affect either the process yield or the fines generated during the granulation.

Fig. 18 shows the product mass fractions as a function of the bed temperature. At relatively high temperatures (but still far away from the melting temperature), coating was the dominant growth mechanism while a combined process of coating/agglomeration took place when the bed was cooled down. Nevertheless, the amount of agglomerates was lower than 8%.

For melt granulation, Boerefijn and Hounslow [16], Seo et al. [21], Tan et al. [22] and Van de Scheur et al. [42], who employed PEG 3000, 4000 or 10000 as binders, reported that below the melting temperature, the agglomeration rate increased as the bed temperature was increased because the high thermal levels retarded the binder solidification. However, Tan et al. [22] also used PEG 1500, finding for this binder a maximum growth rate for temperatures between 32 and 36 °C. In fact, for higher and lower temperatures they observed a decrease of the particle agglomeration rate. The authors indicated that low viscosity binders are easier to spread on the particles surface, promoting a favorable condition for liquid bridge formation, although these bridges are weak at high temperatures reducing the agglomerates formation. Urea melt can be considered as a low viscosity binder (0.0031 Pa s at 135 °C) and therefore, from this point of view, similar to PEG 1500 (0.065 Pa s at 70 °C). Since the viscosity of the urea melt decreases as the bed temperature increases, for similar disruptive forces (i.e. fluidization air velocities), higher probability of liquid bridge rupture are expected at relatively high thermal levels. In fact, as shown in Fig. 18, growth by coating was favored (i.e., event 6 in Fig. 1 prevailed over event 5) at higher bed temperatures within the studied range. It is worth to mention that Tan et al. [22] and Chua et al. [43] showed a decrease in the agglomerates fraction at too low bed temperatures due to less probability of particle-particle contacts at the wet surface, caused by poor binder spreading. This behavior is not observed in the performed urea granulation experiments as a consequence of the relatively high tested bed temperatures. It is also important to note that the above authors performed experiments within an immersion regime, where the particle and droplet sizes are of the same order. In fact, the effect of temperature on the granules growth may differ from a growth regime with droplet sizes much smaller than the particles.

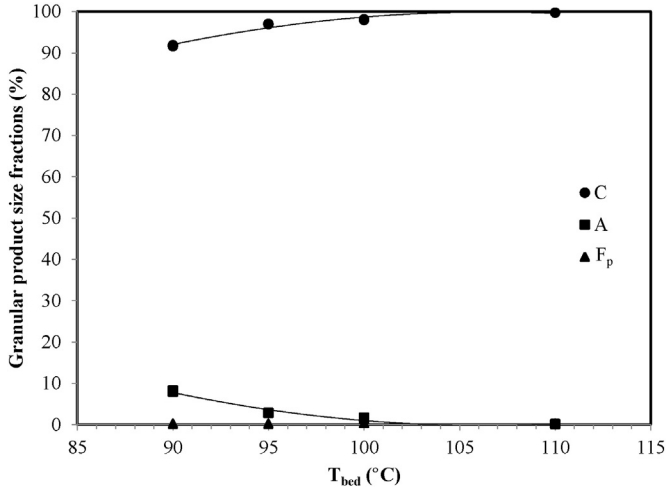

Fig. 18. Case VI. Product mass fractions as a function of the bed temperature.

Again, d_{10} and d_{50} sizes did not change with the variations imposed in this operating variable, being their values identical to those reported for the prior cases. d_{90} increased as the bed temperature decreased accordingly to the agglomerates increased. However, as the maximum agglomerate mass fraction was relatively low, d_{90} changed from 0.38 to 0.36 cm for 90 and 110 °C, respectively (data not shown).

The granules moisture content increased for cooler beds, basically due to the decrease in the evaporation rate. Nevertheless, the moisture content was lower than 0.25 wt.%. As reported by Walker et al. [39] and previously discussed, the crushing strength exhibited an opposite trend; in fact, the granules turned to be more resistant to breakage for relatively high temperatures.

5.6. Effect of the operating variables on the representative diameters

Except for Case V, for all the experiments d_{10} and d_{50} were almost constant and close to 0.27 and 0.31 cm, respectively. As described in Section 4, for a granulation process performed in a perfectly-mixed unit and assuming coating as the only growth mechanism, the number PSD of the granular product corresponds to the number seed distribution but shifted to larger particle sizes. According to Eq. (12) and considering that: a) a constant binder/seed mass ratio was used, b) the granulation efficiency was similar for all the cases and c) the particles growth was by pure coating, the final shifts of the number PSD for all the experiments should be identical. Therefore, if a unique number PSD should be expected for all the experiments governed by coating, a unique mass PSD should also be obtained. Then, for those operating conditions with negligible agglomeration, d_{10}, d_{50} and d_{90} should be almost constant. For Cases I to IV and VI, the experimental results are in good agreement with the theoretical conclusions.

Considering that the seed d_{10} should be close to 0.238 cm and a granulation efficiency of about 90%, Eq. (13) leads to a product $d_{10} =$ 0.277 cm, which is very close to the observed experimental values. The seed d_{50} can be approximated by the seed mean size d_0 (i.e., 0.259 cm), under this assumption the product d_{50} predicted by Eq. (14) becomes 0.30 cm, value that is in good agreement with the experimental data. Summarizing, d_{10} and d_{50} can be successfully predicted by assuming pure coating and a perfectly mixed pattern.

When agglomeration occurred, d_{10} and d_{50} had the same values as for pure coating. This result may be related to the fact that coating was, for all the studied cases, the dominant growth mechanism (i.e., the coated particles accounted for more than 68%). Nevertheless, the formed agglomeration fraction strongly affected d_{90}; which cannot be longer predicted by Eq. (15).

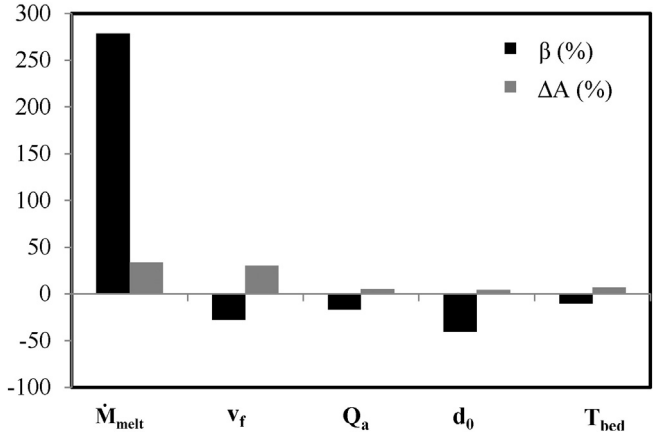

Fig. 19. Studied variables and agglomerate mass fractions changes.

5.7. Operating conditions/seed properties hierarchy of influence on the agglomeration process

The operating variables and seed size were disturbed from the base case to allow agglomeration to appear as a significant growth mechanism. By doing this, different changes were imposed on the selected disturbed variables. Fig. 19 shows the magnitude of these changes, expressed as: $\beta = \frac{V_{max/min} - V_{bc}}{V_{bc}}\ 100$ (V_{bc}: variable value for the base case, $V_{max/min}$: maximum or minimum variable value that led to the maximum amount of agglomerate mass fraction). Therefore, a negative value of β indicates that a decrease in the variable from the base case gave an increase in the agglomerate mass fraction and vice versa. For each variable, Fig. 19 also depicts ΔA, which is defined as the difference between the agglomerate mass fractions for $V_{max/min}$ and V_{bc}. In order to normalize the effect of each variable on the agglomerate formation, Fig. 20 shows, for each studied variable, $\Delta A/\beta$. As it can be seen, the effect of the studied variables on the agglomeration process can be ordered as follows: $v_f > T > Q_a > \dot{M}_{melt} > d_0$.

6. Conclusions

For all the tested process conditions and seed sizes, coating was the main enlargement process (i.e., more than 68% of the granular product were coated particles). For these high levels of coated particles, it was proved that d_{10} and d_{50} were almost identical for all the experiments, regardless of the disturbed operating variable. Considering that a constant binder/seed mass ratio was selected for all the experiments, the observed behavior was explained in terms of the PBE solution for perfectly-mixed systems and pure coating as growth mechanism.

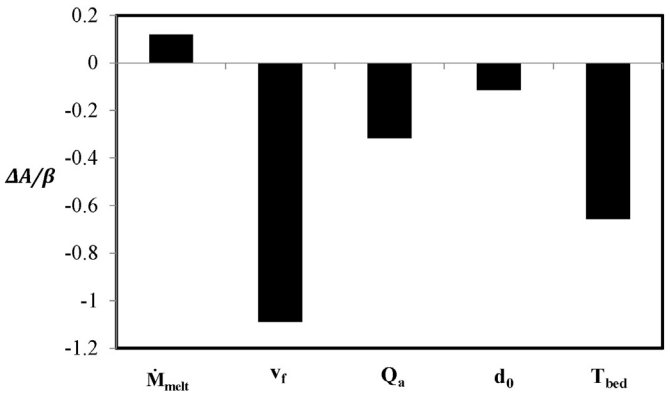

Fig. 20. $\Delta A/\beta$ for each studied variable.

Based on these assumptions, d_{10} and d_{50} were accurately predicted. Even though the mean size remained constant, the PSD span varied significantly for the experiments with noticeable agglomeration. In fact, d_{90} was very sensitive to the enlargement process.

Regarding the influence of the tested variables on the agglomerate formation, the following order of importance was found: $v_f > T > Q_a > \dot{M}_{melt} > d_0$. The agglomeration rate increased as the binder flowrate increased and the fluidization air flowrate, atomization air flowrate and bed temperature decreased. The agglomerated mass fraction presented a non-monotonic behavior as a function of the seed diameter, with a minimum at a seed mean diameter of about 0.26 cm.

Nomenclature

A	agglomerated product mass fraction (%)
A_T	total external surface area of particles (cm^2)
C	pure coated product mass fraction (%)
D_{bot}	granulator bottom diameter (cm)
d_i	particle size (cm)
$\overline{d}_{NV_0}$	seed mean number-volume diameter (cm)
$\overline{d}_{SN_0}$	seed mean surface-number diameter (cm)
D_{top}	granulator top diameter (cm)
d_0	seed arithmetic mean diameter (cm)
d_{10}	particle size corresponding to 10% of the normalized cumulative mass passing function (cm)
d_{10}'	particle size corresponding to 10% of the normalized cumulative number passing function (cm)
d_{50}	particle size corresponding to 50% of the normalized cumulative mass passing function (cm)
d_{50}'	particle size corresponding to 50% of the normalized cumulative number function (cm)
d_{90}	particle size corresponding to 90% of the normalized cumulative mass passing function (cm)
d_{90}'	Particle size corresponding to 90% of the normalized cumulative number passing function (cm)
F'	normalized cumulative number passing function (%)
F_f	filter-bags fines mass fraction (%)
F_{lost}	mass lost fraction (%)
F_p	product fines mass fraction (%)
F_w	wall fines mass fraction (%)
G	coating growth rate (cm/s)
H_{co}	granulator conical section height (cm)
H_{cy}	granulator cylindrical section height (cm)
l	thickness of the liquid layer (cm)
$\dot{M}_{melt}$	urea melt mass flowrate (g/s)
M_{us}	maximum sprayed urea mass (g)
M_{uf}	final urea mass in the bed (g)
M_{u0}	initial urea mass in the bed (g)
N_0	total initial number of seeds (#)
$\dot{Q}_a$	atomization air flowrate (cm^3/s)
T_{melt}	melting temperature (°C)
T_{bed}	bed temperature set-point (°C)
t	time (s)
V_{bc}	variable value for the base case (-)
v_e	air excess velocity (cm/s)
$V_{max/min}$	maximum or minimum variable value (-)
v_{mf}	seed minimum fluidization velocity (cm/s)
v_f	superficial fluidization air velocity (cm/s)
X_u	feed urea mass concentration (wt.%)

Greek symbols

ρ_a	air density (g/cm^3)
μ_a	air viscosity (Poise)
ΔA	difference of the agglomerates mass fractions (%)
γ	granulator angle (°)
η	granulation efficiency (%)

β magnitude of variables changes (%)
ρ_l urea melt density (g/cm^3)
ρ_p urea particle density (g/cm^3)

Subscripts
i Size class *i*
0 Initial

Acknoledgements

FONCyT, CONICET and UNS grants support this study. M.P. Villa thanks CONICET for her doctoral fellowship. The authors also thank Fernanda Cabrera (PLAPIQUI; UNS-CONICET) and Leonardo Mirazú (PROFERTIL S.A.) for their technical assistance.

References

[1] D. Bertín, G. Mazza, J. Piña, V. Bucalá, Modeling of an industrial fluidized-bed granulator for urea production, Ind. Eng. Chem. Res. 46 (2007) 7667–7676, http://dx.doi.org/10.1021/ie070361o.
[2] I.M. Cotabarren, D. Bertín, S. Veliz, L. Mirazú, J. Piña, V. Bucalá, Production of granular urea as nitrogenous fertilizer, in: C.M. Muñoz, A.M. Fernández (Eds.), Urea Synth. Prop. Uses, NOVA Publishers 2012, pp. 1–63.
[3] J.D. Litster, B.J. Ennis, L. Liu, The science and engineering of granulation processes, Particle Technology Series, Kluwer Academic Publishers, Dordrecht, 2004.
[4] S. Heinrich, M. Henneberg, M. Peglow, J. Drechsler, L. Mörl, Fluidized bed spray granulation: analysis of heat and mass transfers and dynamic particle populations, Braz. J. Chem. Eng. 22 (2005) 181–194, http://dx.doi.org/10.1590/S0104-66322005000200004.
[5] K. Saleh, P. Guigon, Coating and encapsulation processes in powder technology, in: A.D. Salman, M.J. Hounslow, J.P.K. Seville (Eds.), Handb. Powder Technol. Elsevier, Amsterdam, The Netherlands, 2007.
[6] H. Zhai, S. Li, D.S. Jones, G.M. Walker, G. Andrews, The effect of the binder size and viscosity on agglomerate growth in fluidised hot melt granulation, Chem. Eng. J. 164 (2010) 275–284, http://dx.doi.org/10.1016/j.cej.2010.08.056.
[7] G.M. Walker, G. Andrews, D.S. Jones, Effect of process parameters on the melt granulation of pharmaceutical powders, Powder Technol. 165 (2006) 161–166, http://dx.doi.org/10.1016/j.powtec.2006.03.024.
[8] J.D. Osborne, R.P.J.J. Sochon, J.J. Cartwright, D.G. Doughty, M.J. Hounslow, A.D. Salman, Binder addition methods and binder distribution in high shear and fluidised bed granulation, Chem. Eng. Res. Des. 89 (2011) 553–559, http://dx.doi.org/10.1016/j.cherd.2010.08.006.
[9] P.G. Smith, A.W. Nienow, Particle growth mechanisms in fluidised bed granulation—I, Chem. Eng. Sci. 38 (1983) 1223–1231.
[10] V. Pont, K. Saleh, D. Steinmetz, M. Hemati, Influence of the physicochemical properties on the growth of solid particles by granulation in fluidized bed, Powder Technol. 120 (2001) 97–104, http://dx.doi.org/10.1016/S0032-5910(01)00355-2.
[11] M. Hemati, R. Cherif, K. Saleh, V. Pont, Fluidized bed coating and granulation: influence of process-related variables and physicochemical properties on the growth kinetics, Powder Technol. 130 (2003) 18–34, http://dx.doi.org/10.1016/S0032-5910(02)00221-8.
[12] S. Iveson, J.D. Litster, K. Hapgood, B.J. Ennis, Nucleation, growth and breakage phenomena in agitated wet granulation processes: a review, Powder Technol. 117 (2001) 3–39, http://dx.doi.org/10.1016/S0032-5910(01)00313-8.
[13] F. Thielmann, M. Naderi, M. Ansari, F. Stepánek, The effect of primary particle surface energy on agglomeration rate in fluidised bed wet granulation, Powder Technol. 181 (2008) 160–168, http://dx.doi.org/10.1016/j.powtec.2006.12.015.
[14] B.J. Ennis, G.I. Tardos, R. Pfeffer, A microlevel-based characterization of granulation phenomena, Powder Technol. 65 (1991) 257–272.
[15] T. Abberger, A. Seo, T. Schaefer, The effect of droplet size and powder particle size on the mechanisms of nucleation and growth in fluid bed melt agglomeration, Int. J. Pharm. 249 (2002) 185–197.
[16] R. Boerefijn, M.J. Hounslow, Studies of fluid bed granulation in an industrial R&D context, Chem. Eng. Sci. 60 (2005) 3879–3890, http://dx.doi.org/10.1016/j.ces.2005.02.021.
[17] H. Zhai, S. Li, G. Andrews, D.S. Jones, S. Bell, G.M. Walker, Nucleation and growth in fluidised hot melt granulation, Powder Technol. 189 (2009) 230–237, http://dx.doi.org/10.1016/j.powtec.2008.04.021.
[18] G.M. Walker, C.R. Holland, M.N. Ahmad, D. Craig, Influence of process parameters on fluidised hot-melt granulation and tablet pressing of pharmaceutical powders, Chem. Eng. Sci. 60 (2005) 3867–3877, http://dx.doi.org/10.1016/j.ces.2005.02.007.
[19] G.M. Walker, S. Bell, G. Andrews, D.S. Jones, Co-melt fluidised bed granulation of pharmaceutical powders: improvements in drug bioavailability, Chem. Eng. Sci. 62 (2007) 451–462, http://dx.doi.org/10.1016/j.ces.2006.08.074.
[20] C. Mangwandi, N.A. Zainal, L. JiangTao, Y. Glocheux, A.B. Albadarin, Investigation of influence of process variables on mechanical strength, size and homogeneity of pharmaceutical granules produced by fluidised hot melt granulation, Powder Technol. 272 (2015) 173–180, http://dx.doi.org/10.1016/j.powtec.2014.11.042.
[21] A. Seo, P. Holm, T. Schæfer, Effects of droplet size and type of binder on the agglomerate growth mechanisms by melt agglomeration in a fluidised bed, Eur. J. Pharm. Sci. 16 (2002) 95–105.
[22] H.S. Tan, A.D. Salman, M.J. Hounslow, Kinetics of fluidised bed melt granulation I: the effect of process variables, Chem. Eng. Sci. 61 (2006) 1585–1601, http://dx.doi.org/10.1016/j.ces.2005.09.012.
[23] P. Heffer, M. Prud'homme, Fertilizer Outlook 2013-2017, 81st IFA Annu. Conf. IFA, Chicago 2013, pp. 20–22.
[24] A. Niks, W. Van Hijfte, R. Goethals, Process for urea granulation, 1980.
[25] A. Kayaert, R. Antonus, Process for the Production of Urea Granules, 5653781, 1997.
[26] D. Bertín, I. Cotabarren, J. Piña, V. Bucalá, Granule size distribution for a multi-chamber fluidized-bed melt granulator: modeling and validation using process measurement data, Chem. Eng. Sci. 104 (2013) 319–329, http://dx.doi.org/10.1016/j.ces.2013.08.012.
[27] K.W. Chua, Y.T. Makkawi, M.J. Hounslow, Time scale analysis for fluidized bed melt granulation I: granule–granule and granule–droplet collision rates, Chem. Eng. Sci. 66 (2011) 318–326, http://dx.doi.org/10.1016/j.ces.2010.10.033.
[28] K.W. Chua, Y.T. Makkawi, B.N. Hewakandamby, M.J. Hounslow, Time scale analysis for fluidized bed melt granulation-II: binder spreading rate, Chem. Eng. Sci. 66 (2011) 327–335, http://dx.doi.org/10.1016/j.ces.2010.10.032.
[29] K.W. Chua, Y.T. Makkawi, M.J. Hounslow, Time scale analysis for fluidized bed melt granulation III: binder solidification rate, Chem. Eng. Sci. 66 (2011) 336–341, http://dx.doi.org/10.1016/j.ces.2010.10.031.
[30] M. Halstensen, P. Debakker, K. Esbensen, Acoustic chemometric monitoring of an industrial granulation production process—a PAT feasibility study, Chemom. Intell. Lab. Syst. 84 (2006) 88–97, http://dx.doi.org/10.1016/j.chemolab.2006.05.012.
[31] H.S. Tan, A.D. Salman, M.J. Hounslow, Kinetics of fluidised bed melt granulation IV. Selecting the breakage model, Powder Technol. 144 (2004) 65–83, http://dx.doi.org/10.1016/j.powtec.2004.05.004.
[32] H.S. Tan, A.D. Salman, M.J. Hounslow, Kinetics of fluidised bed melt granulation V: simultaneous modelling of aggregation and breakage, Chem. Eng. Sci. 60 (2005) 3847–3866, http://dx.doi.org/10.1016/j.ces.2005.02.008.
[33] H.S. Tan, A.D. Salman, M.J. Hounslow, Kinetics of fluidized bed melt granulation—II: modelling the net rate of growth, Chem. Eng. Sci. 61 (2006) 3930–3941, http://dx.doi.org/10.1016/j.ces.2006.01.005.
[34] H.M. Hulburt, S. Katz, Some problems in particle technology, Chem. Eng. Sci. 19 (1964) 555–574, http://dx.doi.org/10.1016/0009-2509(64)85047-8.
[35] A.D. Randolph, M.A. Larson, Theory of Particulate Processes, Academic Press, New York, United States, 1971.
[36] D. Ramkrishna, Population Balances, Academic Press, London, England, 2000.
[37] A. Mahoney, D. Ramkrishna, Efficient solution of population balance equations with discontinuities by finite elements, Chem. Eng. Sci. 57 (2002) 1107–1119, http://dx.doi.org/10.1016/S0009-2509(01)00427-4.
[38] J.C. Strikwerda, Finite Difference Schemes and Partial Differential Equations, Society for Industrial and Applied Mathematics, Philadelphia, USA, 2004.
[39] G.M. Walker, T.R.A. Magee, C.R. Holland, M.N. Ahmad, N. Fox, N.A. Moffatt, Compression testing of granular NPK fertilizers, 1997 231–234.
[40] UNIDO/IFDC (Ed.), Fertilizer Manual, Kluwer Academic Publishers, Dordrecht, The Netherlands, 1998.
[41] C. Srinivasakannan, N. Balasubramaniam, Particle growth in fluidised bed granulation, Chem. Biochem. Eng. 17 (2003) 201–205.
[42] F.T. Van de Scheur, P.L. Goedendorp, A.J. Van der Goot, J.J. Olieman, Fluidised bed agglomeration with polyethylene glycol melt binder: effects of bed temperature and droplet size, World Congr. Part. Technol., Brighton, UK, 1998.
[43] K.W. Chua, Y.T. Makkawi, M.J. Hounslow, A priori prediction of aggregation efficiency and rate constant for fluidized bed melt granulation, Chem. Eng. Sci. 98 (2013) 291–297, http://dx.doi.org/10.1016/j.ces.2013.05.018.